

Room-Temperature Dielectric Switchable Nanocomposites

Peng Meng, Quan Zhang, Yulong Wu, Zhiyuan Tan, Guoan Cheng, Xiaoling Wu, and Ruiting Zheng*

Room-temperature switchable dielectric materials are of interest for many applications, including solar energy storage, smart switches, automatic filters, and next-generation sensors. Here, a temperature-triggered dielectric switchable nanocomposite by dispersing octadecylamine-grafted multiwalled carbon nanotubes (ODA-MWCNTs, for short) into hexadecane is reported. The composite has low permittivity at molten state and high permittivity at frozen state, and the permittivity switch is triggered around 18 °C. The highest permittivity contrast ratio reaches 106.4 at 2.0% CNT volume fraction. The composite shows frequency-sensitive and temperature-ramping-rate-sensitive properties. Further investigation indicates that the permittivity switch is caused by the change of the ODA-MWCNT percolating networks during phase transition.

1. Introduction

Dielectric materials are the building blocks of metal-oxide-semiconductor field-effect transistor,^[1] resonators,^[2] micro-electromechanical systems,^[3] sensors,^[4] and many other devices. The permittivity is a key parameter to reflect the capacitance and polarization of the dielectric materials. The permittivity can be tuned by external stimuli, such as electric field^[5,6] and thermal energy.^[7,8] It provides the opportunity to obtain permittivity switchable materials under different external stimuli. Among them, the room-temperature switchable dielectric materials, which respond automatically around room temperature, have great potentials in many fields, such as solar energy storage, smart switches, automatic filters, next-generation sensors, and so on.

Many works have explored temperature-switchable dielectric materials. “Temperature switchable” means the permittivity of a material changes obviously in a narrow temperature range. In pure polar liquids,^[9] there is a big change of permittivity during liquid–solid phase transition. The permittivity of water


increases from ≈ 2 to ≈ 100 around 273 K. For methanol, the corresponding permittivity changes from ≈ 1 to ≈ 90 at 150 K. Based on polar liquids, Cui et al.^[9] realized the thermal regulation of permittivity from ≈ 7 (100 K) to ≈ 20 (150 K) by the combination of porous coordination polymer $\text{Mn}_2(\text{HCOO})_6$ and polar guest molecules, such as H_2O , CH_3OH , and $\text{C}_2\text{H}_5\text{OH}$. Later, other porous crystals with similar properties, such as $[\text{La}_2\text{Cu}_3\{\text{NH}(\text{CH}_2\text{COO})_2\}_6\cdot(\text{H}_2\text{O})_n]$ and $[\text{Ln}_2\text{Cu}_3(\text{IDA})_6\cdot n\text{H}_2\text{O}]$ were also reported.^[10,11] However, like ceramics,^[12,13] the permittivity of these porous crystals changed continuously; no obvious switch happened near the phase-change points.

Ferroelectric metal organic frameworks (MOFs, for short) caused a great amount of attention in the past decade.^[14–18] The order–disorder phase transition in MOFs triggered by temperature leads to strong variation of dielectric parameters.^[16] Jain et al.^[14] produced cube-shaped $[(\text{CH}_3)_2\text{NH}_2]\text{Zn}(\text{HCOO})_3$ crystals. These crystals showed a permittivity regulation from 3.5 to 16 near 156 K, and the regulation range could be further enlarged by replacing Zn with Mn, Fe, Co, Ni.^[19] Zhang et al.^[20] synthesized $[(\text{CH}_3)_2\text{NH}_2][\text{KCo}(\text{CN})_6]$ crystals, whose permittivity changed between 4 and 19 around 245 K. Zhang et al.^[21] also found that imidazolium periodate (IPI) crystals had a permittivity variation between ≈ 10 (301.6 K) and ≈ 120 (310.2 K). IPI crystal is the first room-temperature switchable dielectric material, and the flexible dielectric switchable thin film was further realized by the compound imidazolium fluorochromate (Im-FCrO₃).^[22] However, the low permittivity contrast ratio and complicated synthesis confined their applications.

In positive temperature coefficient composites, the dielectric or capacitive switchable properties were also reported.^[23–25] However, room-temperature regulation of permittivity was not realized because the soften temperature of the matrix is relatively high. In this work, we present a room-temperature dielectric switchable composite whose permittivity can be regulated around 18 °C. By dispersing a different amount of octadecylamine-grafted multiwalled carbon nanotubes (ODA-MWCNTs, for short) into hexadecane, we obtain dielectric switchable composites with different permittivity contrast. The highest permittivity contrast reaches 106.4. To our best knowledge, it is the highest permittivity contrast ratio at room temperature in existing reports. We also find that microstructural evolution during liquid–solid phase transition is the key to the permittivity switch of composites. The stability and frequency dependence of composites is also studied.

Dr. P. Meng, Dr. Q. Zhang, Dr. Y. L. Wu, Dr. Z. Y. Tan,
Prof. G. A. Cheng, Dr. X. L. Wu, Prof. R. T. Zheng
Key Laboratory of Radiation Beam Technology and Materials
Modification of Ministry of Education
College of Nuclear Science and Technology
Beijing Normal University
Beijing 100875, P. R. China
E-mail: rtzheng@bnu.edu.cn

Prof. G. A. Cheng, Dr. X. L. Wu, Prof. R. T. Zheng
Beijing Radiation Center
Beijing 100875, P. R. China

 The ORCID identification number(s) for the author(s) of this article can be found under <https://doi.org/10.1002/adfm.201701136>.

DOI: 10.1002/adfm.201701136

2. Results and Discussion

2.1. Functionalization of MWCNTs

The chemical oxidation and amidation methods were adopted to improve the compatibility between the MWCNTs and hexadecane.^[26] The surface morphology and chemical states of the MWCNTs were characterized by scanning electron microscopy (SEM), X-ray photoelectron spectroscopy (XPS), and Fourier transform infrared (FT-IR) spectroscopy. From the insets in Figure 1a–c, it is observed that the morphologies of different MWCNTs are similar. However, their surface chemical states are different. The pristine MWCNTs contain some doped O atoms and defects, such as penta/hepta carbon circles on the tube walls. They can be confirmed by the defects (285.1 eV), C–O (286.4 eV), >C=O (287.4 eV) peaks in Figure 1a and the small O peak in Figure 1d. After rigorous treatment in the mixed acid, the C=C bonds of MWCNTs are attacked and broken,^[27] which introduces more O atoms and defects to CNTs, which is confirmed by higher defects peak (285.0 eV) in Figure 1b and the stronger O peak in Figure 1e. The broken C=C bonds are replaced by C–O groups (286.3 eV), >C=O groups (287.4 eV) and –COOH groups (288.8 eV), as shown in Figure 1b. During

the amidation process, ODA-MWCNTs were obtained by the reaction between –COOH groups and ODA molecules. As a proof, the –COOH peak at 288.8 eV in Figure 1c vanishes. As a proof, the –COOH peak at 288.8 eV in Figure 1c vanishes. At the same time, a new peak arises at 288.4 eV, which is believed to be the O=C–N groups. The emergence of new groups results in the content of N atoms increasing, and the consumption of –COOH groups leads to the content of O atoms decreasing sharply, as shown in Figure 1f. The long chain alkanes of ODA molecules grafted on the MWCNTs also enhance the intensity of defects peak (285.0 eV), as shown in Figure 1c. FT-IR spectra of CNTs further confirm our analysis (see Figure S1 in the Supporting Information). All these spectra imply that the ODA molecules are successfully grafted.

2.2. Dielectric Switchable Behavior

Figure 2a shows the typical permittivity switching property of the ODA-MWCNTs/hexadecane composites. The switching occurs between 16.9 and 18.0 °C, which coincides with our previous works.^[26,28,29] Hexadecane is a nonpolar molecule; the low molecular dipole moment determines that its permittivity changes little with temperature. This is proven by the black square dot in

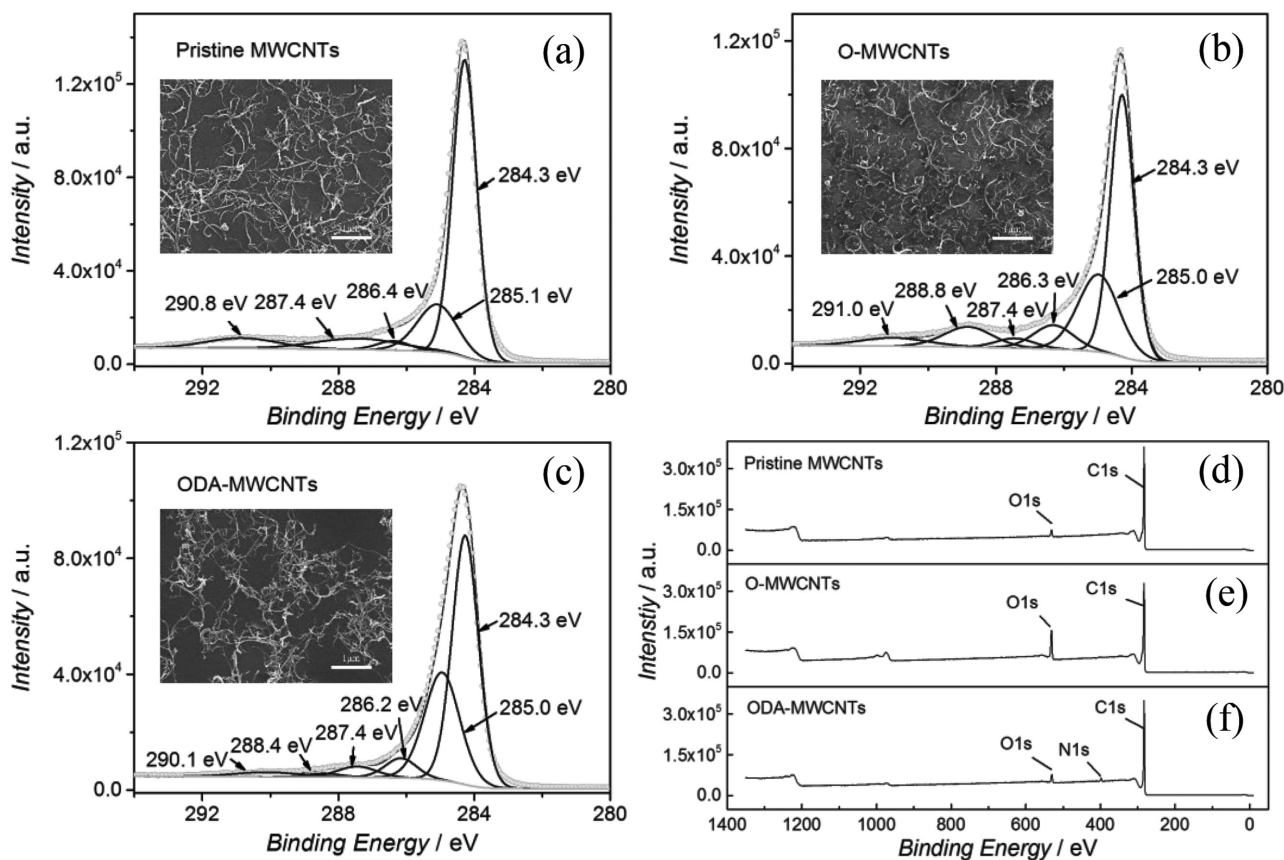


Figure 1. XPS spectra of MWCNTs. a) The C1s deconvoluted spectrum of Pristine MWCNTs, b) the C1s deconvoluted spectrum of O-MWCNTs, and c) the C1s deconvoluted spectrum of ODA-MWCNTs. The gray circle represents the original data, the dark line represents the peaks, the upper gray line represents the envelope results, and the bottom gray line represents the background. The inset is the SEM image of the corresponding sample at 20 K magnification, and its scale bar is 1 μm . d) The XPS survey scan of Pristine MWCNTs, e) the XPS survey scan of O-MWCNTs, and f) the XPS survey scan of ODA-MWCNTs.

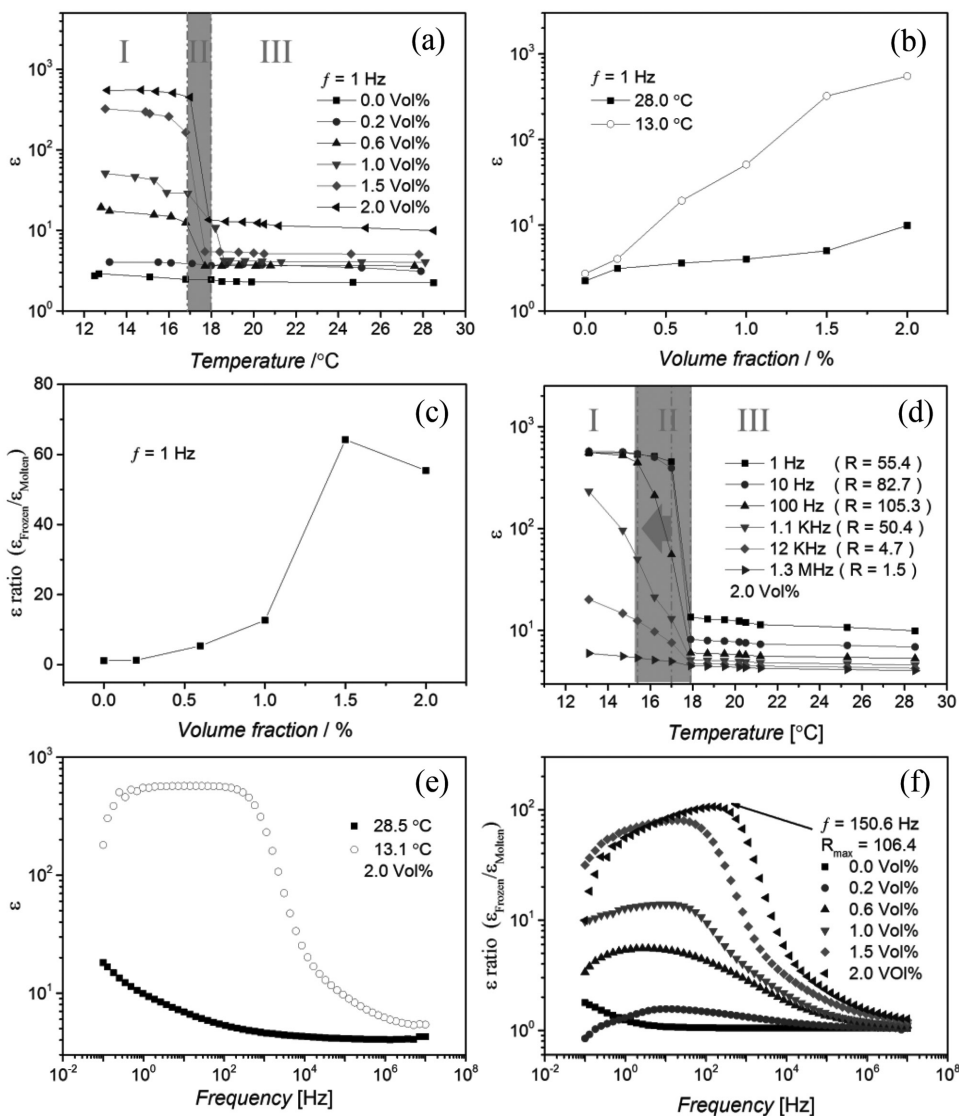


Figure 2. Typical permittivity switching property of the ODA-MWCNTs/hexadecane composites. a) Temperature dependence of the real part of permittivity with different volume fractions at 1 Hz during the phase change. The figure is divided into three regions: I, II, and III. Region I represents the high state, region II represents the jumping area, and the region III represents the low state. b) Volume fraction dependence of the real part of permittivity at 28.0 and 13.0 °C, respectively. c) Volume fraction dependence of ϵ_{ratio} ($\epsilon_{\text{frozen}}/\epsilon_{\text{molten}}$) at 1 Hz. The permittivity switching properties at different frequency are also exhibited. d) Temperature dependence of the real part of permittivity of the 2.0 Vol% sample at different frequency during the phase change. The jumping area (region II) extends as the frequency increases, marked by the gray arrow. The boundary of region II is labeled by the gray dashed line. The ϵ_{ratio} ($\epsilon_{\text{frozen}}/\epsilon_{\text{molten}}$) is marked as R . e) Frequency dependence of the real part of permittivity of the 2.0 Vol% sample at 28.5 and 13.1 °C. f) Frequency dependence of the ϵ_{ratio} ($\epsilon_{\text{frozen}}/\epsilon_{\text{molten}}$) of the different CNT volume fraction samples. The highest ϵ_{ratio} is marked by R_{max} .

Figure 2a. When the temperature is higher than 18.0 °C, hexadecane is a transparent liquid. Lower than 18.0 °C, hexadecane solidifies into needle-like crystals. For the ODA-MWCNTs/hexadecane suspensions, the permittivity “jumps” between 16.9 and 18.0 °C, as highlighted by the gray background (region II). The permittivity increases sharply when the temperature changes from 18.0 to 16.9 °C. When the temperature leaves the “jumping” region, the permittivity shows no significant changes.

The permittivity increases with the increase of CNT volume fraction at 1 Hz frequency, as Figure 2b shows. In liquid state (28.0 °C), the permittivity is 2.2 at 0.0 Vol% and increases

to 9.9 at 2.0 Vol%. In solid state (13.0 °C), the permittivity increases much more quickly with the increase of CNT volume fraction. It changes from 2.7 at 0.0 Vol% to 550.3 at 2.0 Vol%. The variation of permittivity contrast ratio ($\epsilon_{\text{frozen}}/\epsilon_{\text{molten}}$) as a function of CNT volume fraction is shown in Figure 2c. The contrast ratio increases with the increase of CNT volume fraction and reaches the peak (64.2) at 1.5 Vol%. When the volume fraction of CNT further increases to 2.0 Vol%, the permittivity contrast ratio decreases to 55.4. That is because the permittivity of the molten composites increases faster than the frozen composites when the volume fraction is higher than 1.5%.

Besides volume-fraction dependence, the permittivity of composites also shows strong frequency dependence. Figure 2d shows the permittivity switching properties of the 2.0 Vol% sample at different frequency. The trigger temperature still begins at 18.0 °C regardless of the frequency, but the jumping region extends from 1 °C ($f = 1$ Hz) to 3 °C ($f = 1.3$ MHz), as marked by the gray arrow. The switching ratio is frequency-sensitive too. At 1 Hz, the permittivity ratio is 55.4. It increases to 105.3 while the frequency reaches 100 Hz. When the frequency increases to 1.1 kHz, the permittivity ratio decreases to 1.5, which is rather weak. This is caused by the different variation trend of permittivity at different temperature. As shown in Figure 2e, between 0.25 and 150.6 Hz, the permittivity at 13.1 °C keeps a plateau and the permittivity at 28.5 °C undergoes a slow decline. As a result, the switching ratio of 2.0 Vol% sample increases with the frequency, as revealed by the arrow in Figure 2f. At 13.1 °C, the anomalous increase of the permittivity between 0.1 and 0.25 Hz is caused by the short circuit between upper and guard electrode. These data do not reflect the real property of the sample, and will not be discussed in this paper. Beyond 150.6 Hz, the permittivity at 13.1 °C starts to decrease sharply and the permittivity at 28.5 °C becomes stable gradually. As a result, the switching ratio reaches its maximum and then decreases drastically. When the frequency reaches 1.3 MHz, the switching ratio makes no big differences. It is worth mentioning that the dependence of the permittivity on the frequency is common in the CNT-polymer composites.^[30–32] The variation trend of the switching ratio in all samples of this research is shown in Figure 2f. It is found that the higher the volume fraction of the ODA-MWCNTs, the larger the maximum of switching ratio. In the 0.2 Vol% sample, the highest contrast ratio (R_{\max}) is 1.56 at 10.2 Hz. In the 1.5 Vol% sample, the R_{\max} increases to 80.3 at 20 Hz. The largest R_{\max} reaches 106.4 at 150.6 Hz in the 2.0 Vol% sample, as marked by the arrow in Figure 2f. The corresponding switching behavior of the 2.0 Vol% sample is revealed in Figure S2 in the Supporting Information. Its jumping region is located at 15.5–18.0 °C, and the permittivity can be regulated between 550.2 (13.1 °C) and 5.2 (28.5 °C).

2.3. Microstructure Evolution of the Composites during Phase Change

ODA-MWCNTs/hexadecane is a typical conductor–insulator dielectric composite. In such composites,^[33] the permittivity increases sharply as the volume fraction of conductor approaches the percolation threshold. However, it is interesting to find out that the permittivity of solid state is much higher than the permittivity of liquid state in a similar ODA-MWCNTs/hexadecane sample, and the permittivity regulation is completed in a narrow temperature range, as revealed above. In order to reveal the origin of the switchable dielectric behavior, the structure transition during the phase change is studied. Figure 3a–d shows the optical images of the composite with 0.05 Vol% of ODA-MWCNT. At 28.5 °C, the composite is molten. ODA-MWCNTs form small clusters and are uniformly dispersed in liquid, as shown in Figure 3a. The composite freezes when

the temperature falls below 18.0 °C. The microstructure evolution during the process is exhibited in Figure 3b–d. Figure 3b shows the interfaces between the liquid and the solid regions. The ODA-MWCNTs clusters in liquid composite have been squeezed into the grain boundaries^[28] and form ribbon-like aggregations in solid composite, as marked by the dashed box. The ODA-MWCNTs in the aggregations are tensely connected with each other and form good conducting paths. Figure 3c,d presents the lath-like and needle-like crystal area, respectively. Different crystalline morphologies of hexadecane may coexist due to the nonuniform temperature gradients and different nucleation positions in the same sample. In both morphologies, the ODA-MWCNTs ribbon-like aggregation is formed. More details of the optical images can be seen in Figure S3 in the Supporting Information. Figure S3a–c (Supporting Information) shows the different depth-of-focus images of Figure 2b. Figure S3d (Supporting Information) shows the mixed region of the lath-shaped crystals and needle-shaped crystals. When we increase the volume fraction of ODA-MWCNTs, many more aggregations can be formed. These aggregations connect with each other and form percolation networks in the sample. In this way, good conducting networks are built. The schematic diagram is revealed in Figure 3e.

The frequency dependence of conductivity of the 2.0 Vol% sample is shown in Figure 3f. The log–log plots of conductivity versus frequency at 28.5 and 13.1 °C are divided into five distinct regions.^[34] In region I, at low frequency, the electrons are forced to drift over large distances by the alternating electric field. The conductivity corresponds to the DC value and tends to be constant. Due to the loose connection between ODA-MWCNTs at molten state, the conductivity is 3.19×10^{-10} S m⁻¹ at 0.1 Hz. The region I terminates at 0.7 Hz. As the frequency increases, the mean displacement of the electrons is reduced. As a result, the conductivity increases with frequency. In region II, the conductivity follows the power law $\sigma(\omega) \propto \omega^n$ with $0 \leq n \leq 1$.^[35] In region III, the DC conductivity is 8.97×10^{-6} S m⁻¹, which is enhanced by 4 orders of magnitude compared to region I. This is caused by the percolating conducting networks mentioned above. The internal stress between grains reduces the contact resistance between ODA-MWCNTs, which suppresses the resistance in the electrons drifting at low frequency. Besides, the numerous conducting paths provide a better connection between the sample and electrodes. As a result, the sample has higher conductivity. The terminal frequency of region III is about 150.6 Hz. The region IV deviates from the power law. It corresponds to the interfacial relaxation.^[34] The interfacial relaxation or Maxwell–Wagner relaxation is common in heterogeneous systems, such as conductor/insulator composite.^[36] This is caused by the accumulation of electrons on the interface of two phases with significant different permittivities and conductivities. In the solid sample, the electrons accumulated on the interface between the ODA-MWCNTs and the fixed hexadecane molecules. These electrons form large dipoles and lead to interfacial relaxation; however, the interfacial relaxation does not occur between region I and II. This might due to the ambiguous interfaces between ODA-MWCNTs and free hexadecane molecules in liquid composites. These dissociative hexadecane molecules are not able to provide the electrons with stationary and valid accumulating sites. In

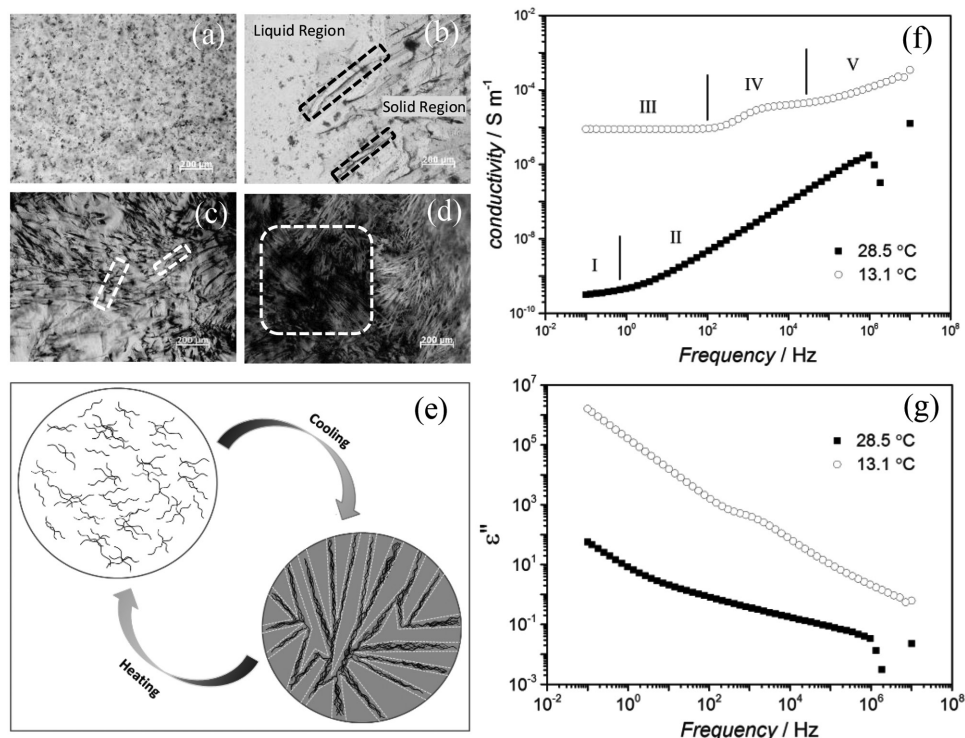


Figure 3. The microstructural evolution and frequency-dependence properties of the ODA-MWCNTs/hexadecane. a) The optical images of molten state ODA-MWCNTs/hexadecane (0.05 Vol%), b) the optical image of liquid/solid boundary, c) the optical image of lath-shaped crystal region, and d) the optical image of needle-shaped crystal region. The scale bar is 200 μm . The squeezed ODA-MWCNTs form ribbon-like aggregations that are remarked by the dashed box. e) The schematic diagram of the repeatable microstructural evolution of ODA-MWCNTs/hexadecane in molten and frozen state. The dark lines represent ODA-MWCNTs, the white background surrounded by the left circle represents the molten hexadecane, the gray background in the right circle represents the frozen hexadecane, and the dotted lines represent the grain boundaries. f) Frequency dependence of the conductivity in the solid (13.1 $^{\circ}\text{C}$) and liquid (28.5 $^{\circ}\text{C}$) ODA-MWCNTs/hexadecane (2.0 Vol%). g) The imaginary part of permittivity varies as a function of frequency in the solid and liquid ODA-MWCNTs/hexadecane (2.0 Vol%).

region V, as the frequency increases, there is not enough time for the electrons to make long-distance migrations and accumulate on the ODA-MWCNTs/hexadecane interfaces. Then, the Maxwell–Wagner relaxation starts to fail. The conductivity follows the power law and increases again.

The percolating conducting networks and interfacial relaxation discussed above also take responsibility for the high permittivity in the solid sample. The percolating conducting networks not only provide numerous interior transportation paths but also act as the geometric extension of the electrode. As a result, abundant electrons are injected from electrodes and make contribution to the capacitance of the sample. Adding the capacitance of the Maxwell–Wagner relaxation, the permittivity of 13.1 $^{\circ}\text{C}$ is much higher than the permittivity of 28.5 $^{\circ}\text{C}$ between 0.25 and 150.6 Hz, as shown in Figure 2e. The high DC conductivity also leads to high dielectric loss, as shown in Figure 3g.^[37] When the electrode injection starts to fail beyond 150.6 Hz, the permittivity also declines sharply, as shown in Figure 2e. Between 150.6 Hz and 30 kHz, the dipoles provided by the interfacial relaxation keeps the permittivity of solid state higher than the liquid state. Beyond 30 kHz, the interfacial relaxation starts to fail, and the permittivity of 13.1 $^{\circ}\text{C}$ gradually approaches the permittivity of 28.5 $^{\circ}\text{C}$.

2.4. Cycling Performance and Switching Performance at Different Temperature Ramping Rate

To investigate the durable performance of the dielectric switch composites, the cycling behavior of 1.5 and 2.0 Vol% ODA-MWCNTs/hexadecane composite is studied, as shown in Figure 4a,b. In order to shorten the measuring period, the experiments are performed at a temperature ramping rate of 15 K h^{-1} . It can be observed that the permittivity of liquid composite (the hollow circle) is low and changes little while the experiment carries on. After solidification, the permittivity (the solid square) becomes high, but decreases in the first six cycles. At 150.6 Hz, the permittivity of 1.5 Vol% sample decreases from 35.1 to 21.7, and the permittivity of 2.0 Vol% sample decreases from 193.9 to 26.8. After that, the permittivity becomes relatively stable, and the switch is repeatable. The permittivity of both molten state and stable frozen state shows a small fluctuation. The fluctuation may come from the imprecise temperature control of the thermostatic water jacket. The repeatability of permittivity comes from the redispersion of ODA-MWCNTs during remelting. The schematic diagram is revealed in Figure 3e. When the hexadecane remelts, the squeezing force disappears. The ODA-MWCNTs are released from the grain boundaries and separate in the liquid because

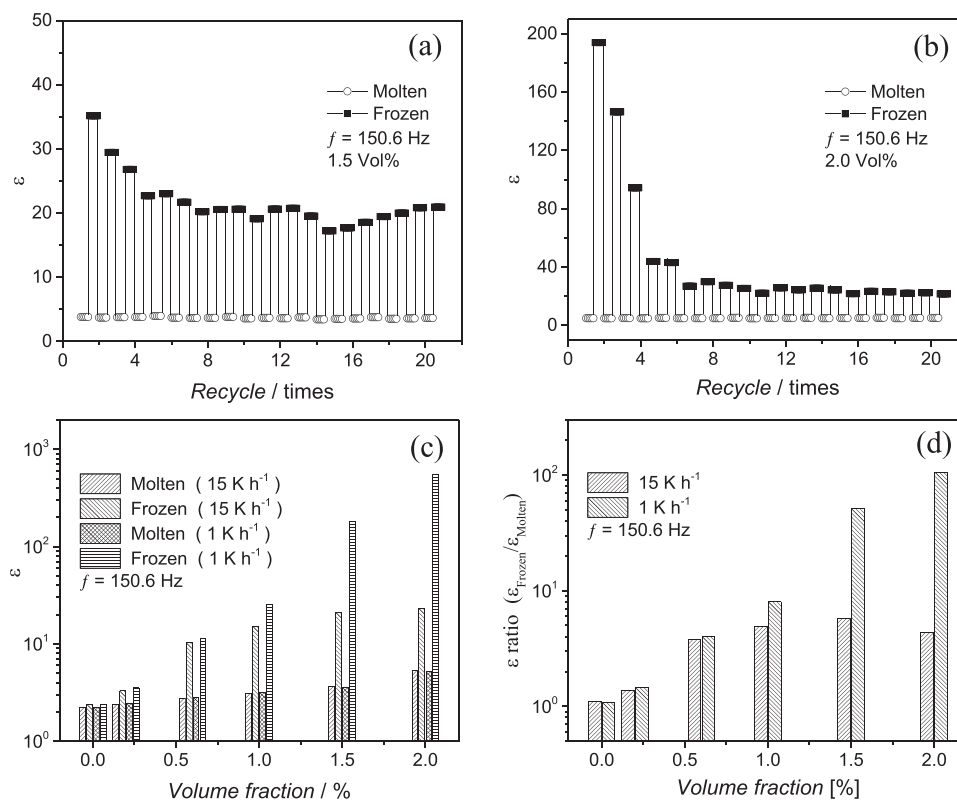


Figure 4. The durable performance of the ODA-MWCNTs/hexadecane composites. The real part of permittivity of the a) 1.5 Vol% and b) 2.0 Vol% sample at 150.6 Hz in 20 cycles. The influence of temperature ramping rate on the switching performance. Volume fraction dependence of c) the real part of permittivity and d) the ϵ_{ratio} ($\epsilon_{\text{frozen}}/\epsilon_{\text{molten}}$) of composites at the different ramping rate of 15 and 1 K h⁻¹ at 150.6 Hz.

of the steric effect of grafted ODA molecules^[26] and Brownian motion. Figure S4a (Supporting Information) shows the molten morphology of the 0.05 Vol% sample after 20 cycles. Compared with Figure 3a, the ODA-MWCNTs recover its dispersion, but the size of the compact cluster is bigger than the initial well dispersed clusters. The larger cluster size reduces the fractal dimension of percolation network under frozen state.^[33] This is the reason for the decrease of permittivity in the first six temperature cycles in solid composites. After that, the size of the clusters become stable,^[26] and the permittivity of composites becomes stable as well. Figure S4b (Supporting Information) shows the frozen morphology of the 0.05 Vol% sample after 20 cycles. The ODA-MWCNTs can always be rearranged in a percolating way as discussed above. The percolating network keeps the permittivity high, and the needle-like grains mean that the crystallization of hexadecane is not influenced by the repetition.

The dielectric performance as a function of CNT volume fraction at different cooling rate is shown in Figure 4c. All data are obtained after 20 cycles (ramping rate = 15 K h⁻¹). The left oblique strip and the grid columns represent the permittivity at molten state, and the right oblique strip and the horizontal stripe columns represent the permittivity at frozen state. Both in liquid and solid composites, the permittivity increases with the increase of CNT volume fraction, regardless of the ramping rate. However, at different ramping rate, the variation trend of permittivity is different. For liquid composites, the ramping

rate does not influence the permittivity. For solid composites, the permittivity at the ramping rate of 1 K h⁻¹ is much higher than that at the ramping rate of 15 K h⁻¹, except for the 0.2 and 0.6 Vol% samples. It leads to the different variation trend of permittivity contrast ratio at different ramping rate, as shown in Figure 4d. The permittivity contrast ratio peaks at 1.5 Vol% (5.7) when the cooling rate is 15 K h⁻¹, and peaks at 2.0 Vol% (106.4) when the cooling rate is 1 K h⁻¹. After 20 cycles, the permittivity switch ratio of 2.0 Vol% ODA-MWCNTs/hexadecane composites still has the 2 orders of magnitude at 1 K h⁻¹ ramping rate, which allow them to have potential applications in smart switches and sensors.

For the 0.2 and 0.6 Vol% samples, the permittivity of solid composites is not sensitive to the temperature ramping rate. This might be due to the low concentration of the filler. When the ODA-MWCNTs are not adequate, the percolation network is hard to regulate by the temperature ramping rate. As a result, the permittivity contrast ratio makes no big difference. When the volume fraction of ODA-MWCNTs is higher than 1.0%, the percolation structure of composites changes a lot between liquid state and solid state, which makes the permittivity contrast ratio sensitive to the ramping rate. The dependence of permittivity on ramping rate can be explained by two possible reasons. The first reason relies on the different crystallization behavior at different cooling rate: the lower cooling rate provides enough time for grains to grow up, which could push more ODA-MWCNTs to the grain boundaries.^[38] On the contrary, at higher cooling

rate, besides accumulating in the boundaries, some ODA-MWCNTs will be engulfed inside the hexadecane crystals. These ODA-MWCNTs make no contribution to the percolating networks.^[38,39] Namely, higher cooling rate reduces the overall permittivity of frozen state by decreasing the effective volume fraction of the conducting component. The second reason is that the crystal formed at lower cooling rate provides a stronger inner stress that squeezes the ODA-MWCNTs more tensely. If the effective volume of the filler is the same, the resistance between ODA-MWCNTs decreases obviously at lower cooling rate. The reduced resistance further enhances the permittivity by improving the electrode injection and interior electron migration as discussed above. In both cases, the lower ramping rate improves the overall conductivity and further enhances the permittivity. The corresponding conductivity is revealed in Figure S5 in the Supporting Information. At 150.6 Hz, the conductivity of composites at the ramping rate of 1 K h⁻¹ is higher than that at the ramping rate of 15 K h⁻¹. It confirms that a better conducting network of ODA-MWCNTs is formed at lower cooling rate in a same sample.

3. Conclusion

In conclusion, we reported a novel room-temperature dielectric switchable material by dispersing ODA-MWCNTs into hexadecane. The switch can be triggered at 18 °C. At the ramping rate of 1 K h⁻¹ and the frequency of 150.6 Hz, the highest switching ratio reaches 106.4 in the 2.0 Vol% sample. The switch is caused by the rearrangement of ODA-MWCNTs in hexadecane matrix during phase transition. During the freezing course, the ODA-MWCNTs are squeezed into the grain boundaries of solid hexadecane to form percolating conducting networks, and the interfaces between ODA-MWCNTs and solid hexadecane give rise to strong Maxwell–Wagner relaxation. These phenomena make the permittivity of the frozen sample increase a lot. All of the volume-fraction-sensitive, frequency-sensitive, and ramping-rate-sensitive properties come from the microstructural change of ODA-MWCNT composites. The switch shows good stability after six temperature cycles, and the switching ratio can be evidently regulated by the change of filler's volume fraction and temperature ramping rate.

4. Experimental Section

Raw Materials: MWCNTs (purity >95wt%, 8–15 nm in outer diameter, 0.5–2 μm in length) were purchased from Chengdu Organic Chemicals Co., China. Nitric acid (65–68 wt%, GR) was bought from Xilong Chemical Co., Ltd., China. Sulfuric acid (95–98 wt%, AR) was bought from Beijing Chemical Works, China. Octadecylamine (ODA, AR) was bought from Sinopharm Chemical Reagent Beijing Co., Ltd., China. Hexadecane (99.56%, GC) was bought from Haltermann, Germany. The deionized water was made in our laboratory. All materials were used without any further purification.

Preparation of Functionalized MWCNTs/Hexadecane Composites: To obtain functionalized MWCNTs, chemical oxidation^[40] and amidation^[41] methods were applied. Typically, 5 g MWCNTs were oxidized in a beaker with 400 mL concentrated H₂SO₄/HNO₃ solution (3:1, V/V) for 24 h. The resultant suspension was rinsed by deionized water and filtered repeatedly until the pH was nearly 7. The obtained carboxylic MWCNTs

(O-MWCNTs) were dried at 60 °C in a vacuum oven for 24 h. Next, the carboxylic MWCNTs were stirred in 450 mL 70 °C SOCl₂ for 24 h. After repeated centrifugation and rinse in tetrahydrofuran, the remaining solids were dried at 40 °C in a vacuum oven for 12 h. Then, the resulting MWCNTs were mixed with 20 g octadecylamine and stirred for 96 h at 95 °C. After cooling to room temperature, the mixture was rinsed in hot ethanol repeatedly until the excess ODA was removed completely. Finally the black slurry was dried at 60 °C in a vacuum oven for 24 h to obtain functionalized MWCNTs (ODA-MWCNTs, for short). The ODA-MWCNTs were dispersed by ultrasonic probe (VCX-750, SONICS) for 60 min at room temperature to obtain liquid composites for dielectric measurements.

Measurements: Dielectric measurements were carried out on an impedance analyzer (Novocontrol GmbH, Hundsangen Germany) in the frequency domain of 0.1 Hz–10 MHz and the temperature range from 10 to 30 °C. Typically, the applied AC voltage was 500 mV. The samples were loaded between two parallel platinum-coated copper disk electrodes of a dielectric measurement cell. The diameter of the electrodes was 30 mm, and the spacing was about 3 mm. The upper electrode was surrounded by a cylindrical guard electrode to shield interference signals. To obtain accurate permittivity and conductivity, the raw experiment data were corrected by the same method in Zhao's works.^[42,43] The accuracy of the measurement results is 0.04%. The temperature of the samples was regulated by a circulating thermostatic water jacket. To shorten the experiment periods, the switchable dielectric properties of the suspensions with different volume fractions were first measured at the temperature ramping rate of about 15 K h⁻¹ for 20 cycles. And then, the fine switching behaviors were investigated at the ramping rate of about 1 K h⁻¹. The accuracy of the temperature is ±0.1 °C.

Structural Characterization: For MWCNTs, the morphologies were investigated by SEM (S-4800, Hitachi). The surface chemical properties of MWCNTs were investigated by XPS (ESCALAB 250 Xi, ThermoFisher) and FT-IR (NEXUS 670, Thermo Nicolet). The cluster structures of ODA-MWCNTs in hexadecane were observed by optical microscope (BX53, Olympus).

Supporting Information

Supporting Information is available from the Wiley Online Library or from the author.

Acknowledgements

The authors thank Prof. K. S. Zhao of the College of Chemistry, Beijing Normal University for the kind help of dielectric measuring and data processing. This work was supported by the National Natural Science Foundation of China (Grant No. 11575025), the Science and Technology Project of Beijing (Grant No. Z171100002017008) and the Fundamental Research Funds for the Central Universities.

Conflict of Interest

The authors declare no conflict of interest.

Keywords

carbon nanotubes, composites, dielectric switches, room temperature materials, phase changes

Received: March 1, 2017

Revised: April 8, 2017

Published online: May 29, 2017

- [1] G. D. Wilk, R. M. Wallace, J. M. Anthony, *J. Appl. Phys.* **2001**, *89*, 5243.
- [2] D. K. Armani, T. J. Kippenberg, S. M. Spillane, K. J. Vahala, *Nature* **2003**, *421*, 925.
- [3] M. Fernandez-Bolanos Badia, E. Buitrago, A. M. Ionescu, *J. Microelectromech. Syst.* **2012**, *21*, 1229.
- [4] Y. Yang, G. Chiesura, T. Vervust, F. Bossuyt, G. Luyckx, J. Degrieck, J. Vanfleteren, *Sens. Actuators, A* **2016**, *243*, 103.
- [5] Y. Liu, R. L. Withers, X. Y. Wei, *Phys. Rev. B* **2005**, *72*, 134104.
- [6] Y. Liu, X. Lu, Y. Jin, S. Peng, F. Huang, Y. Kan, T. Xu, K. Min, J. Zhu, *Appl. Phys. Lett.* **2012**, *100*, 212902.
- [7] J. L. Zhang, P. Zheng, C. L. Wang, M. L. Zhao, J. C. Li, J. F. Wang, *Appl. Phys. Lett.* **2005**, *87*, 142901.
- [8] C. W. Beier, M. A. Cuevas, R. L. Brutchey, *Langmuir* **2010**, *26*, 5067.
- [9] H. B. Cui, K. Takahashi, Y. Okano, H. Kobayashi, Z. Wang, A. Kobayashi, *Angew. Chem., Int. Ed. Engl.* **2005**, *44*, 6508.
- [10] H. Cui, B. Zhou, L.-S. Long, Y. Okano, H. Kobayashi, A. Kobayashi, *Angew. Chem.* **2008**, *120*, 3424.
- [11] B. Zhou, A. Kobayashi, H. B. Cui, L. S. Long, H. Fujimori, H. Kobayashi, *J. Am. Chem. Soc.* **2011**, *133*, 5736.
- [12] Z. Wang, X. M. Chen, L. Ni, X. Q. Liu, *Appl. Phys. Lett.* **2007**, *90*, 022904.
- [13] S. Krohns, P. Lunkenheimer, C. Kant, A. V. Pronin, H. B. Brom, A. A. Nugroho, M. Diantoro, A. Loidl, *Appl. Phys. Lett.* **2009**, *94*, 122903.
- [14] P. Jain, N. S. Dalal, B. H. Toby, H. W. Kroto, A. K. Cheetham, *J. Am. Chem. Soc.* **2008**, *130*, 10450.
- [15] W. Zhang, Y. Cai, R. G. Xiong, H. Yoshikawa, K. Awaga, *Angew. Chem., Int. Ed. Engl.* **2010**, *49*, 6608.
- [16] W. Zhang, R. G. Xiong, *Chem. Rev.* **2012**, *112*, 1163.
- [17] D. W. Fu, H. L. Cai, Y. M. Liu, Q. Ye, W. Zhang, Y. Zhang, X. Y. Chen, G. Giovannetti, M. Capone, J. Y. Li, R. G. Xiong, *Science* **2013**, *339*, 425.
- [18] S. Venkateswarlu, D. Lee, M. Yoon, *ACS Appl. Mater. Interfaces* **2016**, *8*, 23876.
- [19] P. Jain, V. Ramachandran, R. J. Clark, H. D. Zhou, B. H. Toby, N. S. Dalal, H. W. Kroto, A. K. Cheetham, *J. Am. Chem. Soc.* **2009**, *131*, 13625.
- [20] W. Zhang, H. Y. Ye, R. Graf, H. W. Spiess, Y. F. Yao, R. Q. Zhu, R. G. Xiong, *J. Am. Chem. Soc.* **2013**, *135*, 5230.
- [21] Y. Zhang, H. Y. Ye, H. L. Cai, D. W. Fu, Q. Ye, W. Zhang, Q. Zhou, J. Wang, G. L. Yuan, R. G. Xiong, *Adv. Mater.* **2014**, *26*, 4515.
- [22] W.-Y. Zhang, Q. Ye, D.-W. Fu, R.-G. Xiong, *Adv. Funct. Mater.* **2017**, *27*, 1603945.
- [23] F. Bueche, *J. Polym. Sci., Part A-2* **1973**, *11*, 1319.
- [24] F. Bueche, *J. Appl. Phys.* **1973**, *44*, 532.
- [25] Y. Xi, H. Ishikawa, Y. Bin, M. Matsuo, *Carbon* **2004**, *42*, 1699.
- [26] P. C. Sun, Y. L. Wu, J. W. Gao, G. A. Cheng, G. Chen, R. T. Zheng, *Adv. Mater.* **2013**, *25*, 4938.
- [27] J. Zhang, H. L. Zou, Q. Qing, Y. L. Yang, Q. W. Li, Z. F. Liu, X. Y. Guo, Z. L. Du, *J. Phys. Chem. B* **2003**, *107*, 3712.
- [28] R. Zheng, J. Gao, J. Wang, G. Chen, *Nat. Commun.* **2011**, *2*, 289.
- [29] Y. Wu, X. Yan, P. Meng, P. Sun, G. Cheng, R. Zheng, *Carbon* **2015**, *94*, 417.
- [30] L. Wang, Z.-M. Dang, *Appl. Phys. Lett.* **2005**, *87*, 042903.
- [31] Y. Jiao, L. Yuan, G. Liang, A. Gu, *J. Phys. Chem. C* **2014**, *118*, 24091.
- [32] B. Wang, L. Liu, L. Huang, L. Chi, G. Liang, L. Yuan, A. Gu, *Carbon* **2015**, *85*, 28.
- [33] C. W. Nan, Y. Shen, J. Ma, *Annu. Rev. Mater. Res.* **2010**, *40*, 131.
- [34] G. C. Psarras, E. Manolakaki, G. M. Tsangaris, *Composites, Part A* **2003**, *34*, 1187.
- [35] J. C. Dyre, T. B. Schröder, *Rev. Mod. Phys.* **2000**, *72*, 873.
- [36] Z. M. Dang, L. Wang, Y. Yin, Q. Zhang, Q. Q. Lei, *Adv. Mater.* **2007**, *19*, 852.
- [37] J.-K. Yuan, W.-L. Li, S.-H. Yao, Y.-Q. Lin, A. Sylvestre, J. Bai, *Appl. Phys. Lett.* **2011**, *98*, 032901.
- [38] S. N. Schiffrès, S. Harish, S. Maruyama, J. Shiomi, J. A. Malen, *ACS Nano* **2013**, *7*, 11183.
- [39] S. Deville, E. Saiz, R. K. Nalla, A. P. Tomsia, *Science* **2006**, *311*, 515.
- [40] J. Liu, A. G. Rinzler, H. Dai, J. H. Hafner, R. K. Bradley, P. J. Boul, A. Lu, T. Iverson, K. Shelimov, C. B. Huffman, F. Rodriguez-Macias, Y. S. Shon, T. R. Lee, D. T. Colbert, R. E. Smalley, *Science* **1998**, *280*, 1253.
- [41] J. Chen, M. A. Hamon, H. Hu, Y. Chen, A. M. Rao, P. C. Eklund, R. C. Haddon, *Science* **1998**, *282*, 95.
- [42] X. Fan, K. Zhao, *Soft Matter* **2014**, *10*, 3259.
- [43] W. Su, K. Zhao, J. Wei, T. Ngai, *Soft Matter* **2014**, *10*, 8711.